Point and Beam-Sparse Radio Astronomical Source Recovery Using Non-Negative Least Squares

Shahrzad Naghibzadeh*, Ahmad Mouri Sardarabadi*† and Alle-Jan van der Veen*

*Facultuy of EEMCS, Delft University of Technology, Delft, The Netherlands

† Kapteyn Astronomical Institute, University of Groningen, Groningen, The Netherlands

Abstract—A simple and novel algorithm for source recovery based on array data measurements in radio astronomy is proposed. Considering that a radioastronomical image is composed of both point sources and extended emissions, prior information on the images, namely non-negativity and substantial black background are taken into account to choose source representation basis functions. Dirac delta functions are chosen to represent point sources and a Gaussian function approximated from the main beam of the antenna array is selected to capture the extended emissions. We apply the non-negative least squares (NNLS) algorithm to estimate the basis coefficients. It is shown that the sparsity promoted by the NNLS algorithm based on the chosen basis functions results in a super-resolution (finer resolution than prescribed by the main beam of the antenna array pattern) estimate for the point sources and smooth recovery for the extended emissions.

Keywords—Array signal processing, image formation, interferometry, regularization, radio astronomy, non-negative least squares

I. INTRODUCTION

In many array processing and image reconstruction applications, it is required to estimate the location and the intensity of the sources or image pixels given an incomplete and noisy set of measurements from an array of antennas. One such application area is the image formation for radio astronomy in which the goal is to obtain an estimate of the spatial distribution of the intensity of the celestial sources over the field of view (FoV) of the array. In a point source modeling of the radioastronomical imaging problem, the FoV of the array is decomposed in a number of pixels over which the intensity is estimated [1]. Due to the increased sensitivity and larger FoV and the resolution and dynamic range requirements of the current and future radio telescopes, such as the Low Frequency Array (LOFAR) and the Square Kilometer Array (SKA), fine resolution images with a high number of pixels are required. This leads to an underdetermined and ill-conditioned system of equations for the imaging problem for which a regularization scheme is necessary to ensure a unique estimate. Prior information on the radioastronomical images, such as non-negativity and the substantial black background, can be incorporated in the solution method to ensure a unique solution.

Many different iterative techniques have been proposed in the literature for image reconstruction in radio astronomy. The most widely-used technique is the so-called CLEAN method of Högbom [2] which is a sequential source removal technique. At each step of the algorithm, the strongest source position and power are estimated and the effect is removed from the residual image until the residual is noise-like. It has been shown that the CLEAN algorithm is equivalent to a Matching Pursuit (MP) [3] solution method for the ℓ_1-norm constrained minimization of the image pixels [4], [5], [6], [7].

Non-negative least squares (NNLS) were first investigated in the context of radioastronomical imaging by Briggs [8]. Sardarabadi et al. [9] proposed a parallelizable version of the active-set solution method [10] for NNLS and showed the relation between their method and CLEAN. The active-set method acquires a similar technique as CLEAN by iteratively selecting columns from the measurement matrix corresponding to the image pixel with the maximum intensity over the residual image and solving for the intensity by fitting the measurements to the model based on the selected image pixels. The procedure is continued until the residual image reaches a noise-based threshold.

To overcome the deficiency of CLEAN in the presence of extended structures in the image, modifications to the CLEAN algorithm have been proposed [11], [12], [13] which unavoidably compromise the superrresolution characteristics of CLEAN with convergence. Furthermore, Wiaux et al. [14] proposed a method based on the prior of average sparsity of the image over multiple wavelet bases and its parallelized version [15]. These methods suffer from empirical choices of image representation bases and come at an expense of increased computations by sophisticated optimization algorithms.

In this paper, we propose an iterative algorithm for image reconstruction. The prior information about the image that is incorporated in this algorithm are that the radioastronomical image is positive and is composed of both point sources and extended emissions with a substantial black background. We use two basis functions to model the overall image: (i) the Dirac delta function to model the point sources and (ii) a normalized Gaussian function approximated from the main beam of the array pattern. We employ the parallelized version of the active-set method as proposed in [9] to find the non-negative coefficients of the selected bases in each iteration. We show that in each iteration, the proposed algorithm performs a similar procedure as matched filtering on the residual image to select the basis and the corresponding pixel with the maximum contribution in the residual image. The data is fit to the model based on the selected image pixels in a least squares sense and the iteration is terminated when the residual image reaches a predefined noise threshold. The performance of the proposed method is evaluated using numerical simulations.

II. DATA MODEL

We explain the array processing framework and the data model employed for radioastronomical image reconstruction. Similar to the notations suggested in [1] and [9], $(.)^T, (.)^H, (.)^*, \circ, \otimes$ and $(.)^\odot$ respectively denote transpose, the Hermitian transpose, complex conjugate, Khatri-Rao product, the Kronecker product and element-wise power. The antenna array under consideration is composed of P distinct receiving elements and assuming a discrete point source model [1], the FoV of the array is discretized into Q pixels or grid points denoting potential point source positions.

The celestial sources are assumed to be stationary. Due to the earth-bound positions of the antenna array elements

and the rotation of the earth, the observation time of the celestial sources is divided into a number of time snapshots over which the observed position of the celestial sources are considered stationary. The received signals on each antenna element and over each time snapshot k are first time-sampled into N samples and divided into narrow frequency bands. The sampled received signals on all the array elements for one frequency band is represented as

$$\mathbf{y}_k[n] = \mathbf{A}_k\mathbf{s}[n] + \mathbf{n}_k[n], \ n = 1, \cdots, N. \tag{1}$$

In this representation, $\mathbf{y}_k[n]$, $\mathbf{s}[n]$ and $\mathbf{n}_k[n]$ respectively denote the $P \times 1$ vector of the received signal sample over all the antennas, the $Q \times 1$ vector of the sampled source signals and the $P \times 1$ vector indicating the sampled noise signal on all the receivers. $\mathbf{A}_k$ is the $P \times Q$ array response matrix. In the rest of the paper we consider a single time snapshot and frequency band and therefore drop the index k. The formulation can readily be extended to multiple snapshots and frequencies. Denoting the array response matrix in terms of its columns as $\mathbf{A} = [\mathbf{a}_1, \mathbf{a}_2, \mathbf{a}_3, \cdots, \mathbf{a}_Q]$, each column represents the response of the array towards the corresponding pixel in the image plane. Furthermore, each element of the array response matrix is computed as

$$a_{p,q} = \frac{1}{\sqrt{P}} e^{-j\frac{2\pi}{\lambda}\mathbf{v}_p^T\mathbf{z}_q} \tag{2}$$

where λ is the wavelength of the received radio frequency signal , $\mathbf{v}_p$ is a 3×1 vector of the Cartesian location of the pth array element with respect to a chosen origin in the field of array and $\mathbf{z}_q$ contains the direction cosines of the qth pixel in the image plane. The receiver noise and the astronomical signals can be assumed to have a Gaussian distribution due to the central limit theorem. Therefore, covariance matrices provide sufficient statistics for the received signals [16]. Assuming the signals and the receiver noise are uncorrelated, the autocovariance of the received signals is indicated as [1]

$$\mathbf{R} = E\{\mathbf{y}[n]\mathbf{y}^H[n]\} = \mathbf{A}\boldsymbol{\Sigma_s}\mathbf{A}^H + \boldsymbol{\Sigma_n}, \tag{3}$$

where $\boldsymbol{\Sigma_s} = \text{diag}\{\boldsymbol{\sigma}\}$ and $\boldsymbol{\Sigma_n} = \text{diag}\{\boldsymbol{\sigma_n}\}$ represent the covariance matrices associated with the source signals and the received noise respectively. An estimate of the data covariance matrix is obtained using the available received data samples. The sample covariance matrix is calculated as

$$\hat{\mathbf{R}} = \frac{1}{N}\sum_{n=1}^{N}\mathbf{y}[n]\mathbf{y}^H[n]. \tag{4}$$

The measurement equation is obtained by vectorizing the covariance data model and the covariance measurement data

$$\hat{\mathbf{r}} = \mathbf{r} + \mathbf{w}, \tag{5}$$

where $\hat{\mathbf{r}} = \text{vec}(\hat{\mathbf{R}})$, $\mathbf{r} = \mathbf{M}\boldsymbol{\sigma} + \mathbf{r_n}$, in which $\mathbf{M} = \mathbf{A}^* \circ \mathbf{A}$ and $\mathbf{r_n} = \text{vec}(\boldsymbol{\Sigma}_n) = (\mathbf{I} \circ \mathbf{I})\boldsymbol{\sigma_n}$, and $\mathbf{w}$ is zero-mean additive noise with covariance [17]

$$\text{Cov}(\mathbf{w}) = E\{(\hat{\mathbf{r}} - \mathbf{r})(\hat{\mathbf{r}} - \mathbf{r})^H\} = \frac{1}{N}(\mathbf{R}^* \otimes \mathbf{R}). \tag{6}$$

III. PROBLEM STATEMENT

Based on the data model presented in the previous section, the imaging problem reduces to estimating the celestial source powers, indicated in a discretized form as $\boldsymbol{\sigma} = [\sigma_1, \sigma_2, \sigma_3, \cdots, \sigma_Q]^T$, from the received noisy and incomplete covariance data $\hat{\mathbf{r}}$. Assuming the knowledge of the noise covariance vector $\mathbf{r_n}$, we can subtract the effect form $\hat{\mathbf{r}}$.

If the noise variance vector $\boldsymbol{\sigma_n}$ is not known, it can be estimated together with the image pixels as explained in [1]. In the following formulation we ignore $\mathbf{r_n}$. The measurement matrix $\mathbf{M}$ relates the covariance measurements to the desired source powers. The columns of matrix $\mathbf{M}$ are constructed from the columns of the array response matrix $\mathbf{A}$ as $\mathbf{M} = [\mathbf{a}_1^* \otimes \mathbf{a}_1, \mathbf{a}_2^* \otimes \mathbf{a}_2, \mathbf{a}_3^* \otimes \mathbf{a}_3, \cdots, \mathbf{a}_Q^* \otimes \mathbf{a}_Q]$. In high-resolution imaging, the number of image pixels is very large [18]. We formulate the imaging problem as a high-dimensional least squares regression problem with non-negativity constraints on the source powers as

$$\underset{\boldsymbol{\sigma}}{\text{minimize}} \parallel \hat{\mathbf{r}} - \mathbf{M}\boldsymbol{\sigma} \parallel_2^2, \text{ subject to } \boldsymbol{\sigma} \geqslant \mathbf{0}. \tag{7}$$

In this problem formulation, the available covariance data is fit to the model in a LS sense such that the residual $\hat{\mathbf{r}} - \mathbf{M}\boldsymbol{\sigma}$ is minimized. In high-resolution imaging, matrix $\mathbf{M}$ is a wide matrix and the aforementioned least squares problem is underdetermined. Therefore, an infinite number of solutions are possible. To obtain a unique solution, regularization is necessary. Non-negativity constraint restricts the space of the possible solutions to only non-negative solutions. Furthermore, due to the presence of substantial black background in radioastronomical images, most of the pixels in $\boldsymbol{\sigma}$ have near zero value and need not be estimated. The NNLS algorithm naturally incorporates this assumption in the solution method as will be explained.

The gradient vector of the cost function in Equation 7 is $\mathbf{M}^H(\mathbf{M}\boldsymbol{\sigma} - \hat{\mathbf{r}})$ and must vanish at the optimum for an unconstrained problem [19]. The active-set algorithm for NNLS [10] iteratively reduces the residual image, which is the negative of the gradient vector, until it converges to the noise threshold vector of the image, $\boldsymbol{\epsilon}$. The image is initialized by an all-zero vector $\boldsymbol{\sigma}^{(0)} = \mathbf{0}$ (the black background). In each iteration of the algorithm, the residual image is computed based on the current estimate of the image, $\boldsymbol{\sigma}^{(i)}$, and its maximum is found. The image pixels are split into two sets in each step, one set of pixels that are kept at 0 is called the active set, denoted by $\mathcal{A}$, and the second set is composed of the image pixels that are free to vary and therefore are called the free set, indicated by $\mathcal{F}$. The location of the maximum of the gradient vector at iteration i corresponds to a potential source location. Therefore, the corresponding pixel is moved from the active set to the free set and the minimization problem

$$\underset{\boldsymbol{\sigma}_{\mathcal{F}}}{\text{minimize}} \parallel \hat{\mathbf{r}} - \mathbf{M}_{\mathcal{F}}\boldsymbol{\sigma}_{\mathcal{F}}^{(i)} \parallel_2^2$$

is solved for all the pixels in the free set, $\boldsymbol{\sigma}_{\mathcal{F}}$, to estimate their intensity. In this equation, $\mathbf{M}_{\mathcal{F}}$ only contains the columns of $\mathbf{M}$ corresponding to the pixels in the free set. The solution to the aforementioned problem is checked for positivity and if the constraint is violated additional steps are performed to ensure the feasibility of the solution [10].

As can be seen, by iteratively selecting the columns of $\mathbf{M}$ and with the underlying assumption of the sparsity of the sources in a black background in the image, active-set performs a sparsity-promoting regularization because most of the columns of $\mathbf{M}$ correspond to zero pixel values and remain in the active set. Furthermore, the gradient calculation and maximum selection is similar to performing a matched-filtering on the residual vector $\hat{\mathbf{r}} - \mathbf{M}\boldsymbol{\sigma}^{(i)}$ at the ith iteration. It was shown that the NNLS algorithm obtains good position and intensity estimates in scenarios where the underlying image is composed of a sparse set of point sources [8], [9]. However, the convergence rate and the intensity estimates are adversely affected in scenarios where extended emissions are present.

IV. THE PROPOSED ALGORITHM

In order to tackle the aforementioned problems in the presence of extended emissions as well as point sources, we propose to represent the image in a dual basis form as

$$\boldsymbol{\sigma} = \boldsymbol{\Phi}\boldsymbol{\alpha}, \text{ where } \boldsymbol{\Phi} = [\mathbf{I}, \mathbf{B}]. \tag{8}$$

In this formulation, $\boldsymbol{\Phi}$ is a $Q \times 2Q$ matrix that is composed of two $Q \times Q$ matrices $\mathbf{I}$ and $\mathbf{B}$. $\mathbf{I}$ is the identity matrix that represents pixel basis for the recovery of point sources. We choose this basis to retain the super-resolution point source recovery feature of the NNLS algorithm. We propose to capture the extended emissions with the actual resolution of the antenna array. For this purpose, we choose a Gaussian function with the same Full Width at Half Maximum (FWHM) as the Half Power Beam Width (HPBW) of the antenna array. Each column of $\mathbf{B}$ is a shifted version of the aforementioned Gaussian function with the peak shifted to the location of the corresponding pixel and normalized such that the total underlying energy is 1.

With the choice of a positive basis matrix $\boldsymbol{\Phi}$, we restrict our attention to the positive coefficient set $\boldsymbol{\alpha}$. Therefore, we can reformulate the image reconstruction problem as

$$\underset{\boldsymbol{\alpha}}{\text{minimize}} \parallel \hat{\mathbf{r}} - \mathbf{M}\boldsymbol{\Phi}\boldsymbol{\alpha} \parallel_2^2, \text{ subject to } \boldsymbol{\alpha} \geqslant \mathbf{0}. \tag{9}$$

This problem is underdetermined and leads to an infinite set of feasible solutions. We apply the modified active-set algorithm to the aforementioned problem to recover the basis coefficients $\boldsymbol{\alpha}$. The proposed algorithm works on the implicit assumption of the sparsity of the signal over the predefined basis to obtain a unique solution. The authors in [20] have investigated the similarity of the active-set algorithm with the orthogonal matching pursuit algorithm [21] in terms of sparse recovery. We call this new method the dual-basis non-negative least squares as explained in Algorithm 1.

As illustrated in Algorithm 1, we begin with an empty sky (zero basis coefficients). Therefore, all of the indices are in the active set $\mathcal{A}$ and the free set is empty. The initial residual basis coefficient vector is computed in step 2 as $\Delta\boldsymbol{\alpha} = \boldsymbol{\Phi}^H\mathbf{M}^H(\hat{\mathbf{r}} - \mathbf{M}\boldsymbol{\Phi}\boldsymbol{\alpha})$. In fact $\Delta\boldsymbol{\alpha}$ represents the matched filter output power projected in the basis coefficient space. The stopping criteria for the algorithm as explained in step 3 are when there are no more indices in the active set or when all of the indices in the residual coefficient vector $\Delta\boldsymbol{\alpha}$ have reached the corresponding detection threshold. In order to choose the pixel-based detection threshold ϵ, based on Equation 6, when all the sources are estimated the covariance of the residual basis coefficient vector is

$$\text{Cov}(\Delta\boldsymbol{\alpha}) = \frac{1}{N}\boldsymbol{\Phi}^H\mathbf{M}^H(\mathbf{R}^* \otimes \mathbf{R})\mathbf{M}\boldsymbol{\Phi}. \tag{10}$$

To set the detection threshold, we compute an estimate of the standard deviation of the residual basis coefficient vector based on the available data $\hat{\mathbf{R}}$ and allow for a false alarm rate of 0.01 %. Therefore, for the $2Q \times 1$ vector of index-based detection threshold we have

$$\boldsymbol{\epsilon} = 6 \times \frac{1}{\sqrt{N}}(\text{vecdiag}(\boldsymbol{\Phi}^H\mathbf{M}^H(\hat{\mathbf{R}}^* \otimes \hat{\mathbf{R}})\mathbf{M}\boldsymbol{\Phi}))^{\odot\frac{1}{2}}. \tag{11}$$

At step 4 of the algorithm, the coefficient corresponding to the maximum output power of the matched filter projected in the coefficient space is computed. This is the step that explains the key idea of the proposed method. The maximum not only shows the location (Direction of Arrival, DoA) of the potential source but it also provides the most likely shape of the source

---

Algorithm 1: Dual-basis non-negative least squares

input : $\hat{\mathbf{r}}$,M,$\boldsymbol{\Phi}$,$\boldsymbol{\epsilon}$
output: Basis coefficient vector $\boldsymbol{\alpha}$

1 Initialize: $\mathcal{F} = \varnothing$, $\mathcal{A} = \{1, 2, 3, \cdots, 2Q\}$ and $\boldsymbol{\alpha} = \mathbf{0}$;
2 Compute the initial residual basis coefficient vector $\Delta\boldsymbol{\alpha} = \boldsymbol{\Phi}^H\mathbf{M}^H(\hat{\mathbf{r}} - \mathbf{M}\boldsymbol{\Phi}\boldsymbol{\alpha})$;
3 **while** $\mathcal{A} \neq \varnothing$ *and* $\Delta\alpha_t > \epsilon_t$ *for any* $t \in \mathcal{A}$ **do**
4     $m = \underset{t}{\text{argmax}}\{\Delta\alpha_t \mid t \in \mathcal{A}\}$;
5   add m to $\mathcal{F}$ and remove from $\mathcal{A}$;
6   Solve for the coefficients in the set $\mathcal{F}$
     $\boldsymbol{\beta}_{\mathcal{F}} = \underset{\boldsymbol{\alpha}_{\mathcal{F}}}{\text{argmin}} \parallel \hat{\mathbf{r}} - \mathbf{M}_{\mathcal{F}}\boldsymbol{\Phi}_{\mathcal{F}}\boldsymbol{\alpha}_{\mathcal{F}} \parallel_2^2$;
7   Define $\beta_n := 0$ for $n \in \mathcal{A}$;
8   **if** $\beta_u \leqslant \epsilon_u$ *for any* $u \in \mathcal{F}$ **then**
9   **while** $\beta_u \leqslant \epsilon_u$ *for any* $u \in \mathcal{F}$ **do**
10        $h = \text{argmin}\frac{\alpha_u}{\alpha_u - \beta_u}$ for $u \in \mathcal{F}$, $\beta_u \leqslant \epsilon_u$;
11   Set $\delta = \frac{\alpha_h}{\alpha_h - \beta_h}$;
12   Set $\boldsymbol{\alpha} = \boldsymbol{\alpha} + \delta(\boldsymbol{\beta} - \boldsymbol{\alpha})$;
13   Move from $\mathcal{F}$ to $\mathcal{A}$ all indexes s for which $|\alpha_s| < \epsilon_s$;
14   Repeat steps 6 and 7;
15   **end**
16   **else**
17   Set $\boldsymbol{\alpha} = \boldsymbol{\beta}$;
18   Compute $\Delta\boldsymbol{\alpha} = \boldsymbol{\Phi}^H\mathbf{M}^H(\hat{\mathbf{r}} - \mathbf{M}\boldsymbol{\Phi}\boldsymbol{\alpha})$
19   **end**
20 **end**

---

by choosing the coefficient in the basis that maximizes the output power. This way, we can distinguish between point sources and extended sources and estimate the source power in the next steps based on the chosen basis as done in step 6. The regularized minimization problem in step 6 is solved by an iterative algorithm such as LSQR [22]. Steps 8 to 14 check if all of the computed coefficients in the free set satisfy the corresponding bound. If the bound is violated for some of the coefficients, the maximum step size, δ, towards the bound is found and the coefficients and the sets are updated accordingly in step 11 and 12. Afterwards, the minimization in step 6 is recomputed until all of the coefficients in the free set satisfy the bound, after which the residual basis coefficients are recomputed in step 12 and the iteration is continued until convergence is reached.

V. NUMERICAL RESULTS AND PERFORMANCE ANALYSIS

We consider a one-dimensional test example to evaluate the performance of the proposed algorithm. A random non-uniform linear array with $P = 30$ antenna elements is considered. The FoV of the array in terms of the θ angle is in the range $(-90°, 90°)$. The wavelength of the radio frequency is chosen to be $\lambda = 2$ m. Assuming the placement of the antenna elements on the x axis and indicating the position of the pth antenna element as x_p, the beam pattern of the antenna array is calculated as

$$f(l_q) = \frac{1}{P}\sum_{m=1}^{P}\sum_{p=1}^{P}e^{-j\frac{2\pi}{\lambda}(x_m - x_p)l_q}. \tag{12}$$

The maximum of the beam pattern is P and the half power beam width of the array is approximately HPBW $\approx \frac{\lambda}{\Delta x_{max}}$ radians [23] where Δx_{max} is the maximum distance between all
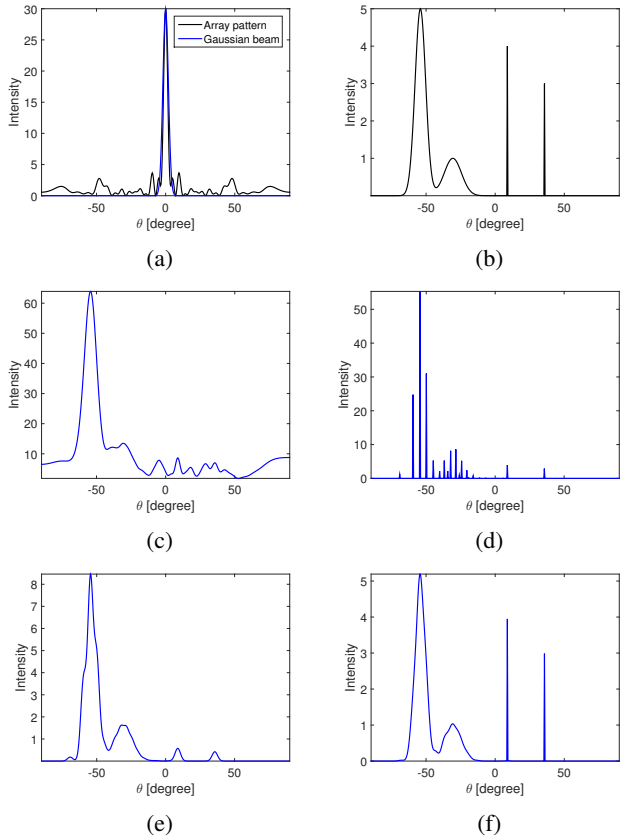
Fig. 1: (a) Array pattern and the Gaussian fit, (b) The underlying source intensity distribution (c) Matched-filter dirty image, (d) Recovered image based on the NNLS algorithm, (e) Gaussian beam applied on the result of NNLS and (f) Recovered image based on the dual-basis NNLS algorithm.

of the antenna pairs. This indicates the resolution of the system. The image resolution is chosen as $\Delta\theta = 0.1 \times HPBW \approx 0.4°$; Therefore, the number of image pixels is $Q = 429$. The direction cosine on the sky for the qth pixel is computed as $l_q = \sin\theta_q$ [24]. We fit a Gaussian function to the main beam of the array. The Gaussian function with the same maximum amplitude as the beam pattern function centered at zero is

$$g(l_q) = P \exp\left(\frac{l_q^2}{2\rho^2}\right), \ q = 1, 2, 3, \cdots, Q. \tag{13}$$

The FWHP for the Gaussian function happens at $2\rho\sqrt{2\ln 2}$. Setting $\lambda/\Delta x_{max} = 2\rho\sqrt{2\ln 2}$, the width of the Gaussian to fit the main beam of the array is $\rho = \frac{\lambda}{2\Delta x_{max}\sqrt{2\ln 2}}$. An instance of the non-uniform linear array and the corresponding array beam pattern and the Gaussian function fit to its main beam is shown in Figure 1. We then normalize this Gaussian function such that the contained energy over all the discrete points is summed to 1. The array beam pattern and the Gaussian fit are shown in Figure 1(a).

To investigate the performance of the proposed algorithm, we apply the algorithm on the aforementioned non-uniform linear array. The underlying source intensities and the matched-filtered dirty image are shown in Figure 1(b) and (c). The sources are composed of two point sources with the intensities 4 and 3 placed at the angles $8.8°$ and $35.6°$ respectively and two Gaussian sources with the peak intensities 5 and 1 with different widths placed respectively at the angles $-54.1° -30.6°$.

Number of antennas	20	30	40	50
Number of pixels	303	429	611	757
Computation time NNLS	0.53	0.67	1.47	4
Dual-basis NNLS	0.34	0.69	1.46	3.25
Number of iterations NNLS	20.73	21.68	27.5	39.55
Dual-basis NNLS	15.49	20.26	24.05	31
Basis elements NNLS	19.73	20.52	26.5	37.57
Dual-basis NNLS	10.69	18.39	22.05	28.5
Error norm NNLS	54.36	66.5	79.92	72.83
Post-processed NNLS	21.74	14.36	7.4	5.1
Dual-basis NNLS	1.08	0.75	1.49	1.42

TABLE I: Performance analysis

To construct the sampled covariance matrix, Gaussian receiver noise with variance $\sigma_n = 0.5$ is added to the covariance $\mathbf{R}$ and $N = 10^5$ data samples are used to construct the sample covariance matrix $\hat{\mathbf{R}}$. The image obtained by applying the NNLS algorithm is shown in Figure 1(d). As can be seen, the extended sources are approximated by a large number of point sources and the intensity estimates are much larger than the actual intensities. Figure 1(e) shows the result of convolving the result of NNLS with the normalized Gaussian beam times the pixel width. This post processing retains the shape of the extended sources at the expense of reducing the resolution of point sources; Furthermore, the intensity estimates are still not correctly restored. Figure 1(f) shows the result of applying the proposed dual-basis NNLS algorithm. As can be seen, both the extended emissions and the point sources are estimated correctly with super-resolution estimate of the point sources and the intensity estimates are very close to the true intensities.

The performance of the dual-basis NNLS algorithm was compared to the performance of the NNLS algorithm and the post-processed version of NNLS by running the algorithms for 100 noise instances for random linear arrays with different number of elements. The pixel resolution was kept at 0.1 of the main beam of the array. Table I displays the number of antenna elements, the associated number of pixels, the algorithm computation time in seconds, the number of iterations until convergence to the threshold, the number of non-zero elements needed to represent the sources and the average error norm $\| \boldsymbol{\sigma} - \hat{\boldsymbol{\sigma}} \|_2 / 100$. Based on the results of the experiments, we conclude that by applying the dual-basis NNLS algorithm we are able to capture the actual intensity of both point sources and extended emissions with a small number of basis elements with high accuracy. Furthermore, the number of iterations and computing time are decreased with respect to NNLS.

VI. CONCLUSIONS

Array processing for radioastronomical source recovery was investigated in this paper. To capture both extended emissions and point sources with high resolution, we proposed a dual-basis NNLS algorithm. In this method the super-resolution point source recovery was retained by a Dirac delta function as a basis for point source representation and the actual resolution of the antenna array was restored by a normalized Gaussian beam as a basis for extended source recovery. By simulations on a one dimensional test example we showed the super-resolution point source recovery as well as good approximation of the extended emissions. Furthermore, the increased sparsifying regularization obtained by applying the dual-basis NNLS and the performance of the algorithm in terms of estimation error, number of iterations and running time was investigated by Monte-Carlo simulations on random linear arrays with different number of antennas.

REFERENCES

[1] A.-J. van der Veen and S. J. Wijnholds, "Signal processing tools for radio astronomy," in *Handbook of Signal Processing Systems*. Springer, 2013, pp. 421–463.

[2] J. Högbom, "Aperture synthesis with a non-regular distribution of interferometer baselines," *Astronomy and Astrophysics Supplement Series*, vol. 15, p. 417, 1974.

[3] S. G. Mallat and Z. Zhang, "Matching pursuits with time-frequency dictionaries," *Signal Processing, IEEE Transactions on*, vol. 41, no. 12, pp. 3397–3415, 1993.

[4] K. Marsh and J. Richardson, "The objective function implicit in the CLEAN algorithm," *Astronomy and Astrophysics*, vol. 182, pp. 174–178, 1987.

[5] R. Levanda and A. Leshem, "Radio astronomical image formation using sparse reconstruction techniques," in *IEEE 25th convention of Elec. Electron. Eng. in Israel (IEEEI 2008)*, 2008, pp. 716–720.

[6] Y. Wiaux, L. Jacques, G. Puy, A. Scaife, and P. Vandergheynst, "Compressed sensing imaging techniques for radio interferometry," *Monthly Notices of the Royal Astronomical Society*, vol. 395, no. 3, pp. 1733–1742, 2009.

[7] L. C. Schwardt, "Compressed sensing imaging with the kat-7 array," in *Electromagnetics in Advanced Applications (ICEAA), 2012 International Conference on*. IEEE, 2012, pp. 690–693.

[8] D. S. Briggs, *High fidelity deconvolution of moderately resolved sources*. D. Briggs, 1995.

[9] A. M. Sardarabadi, A. Leshem, and A.-J. van der Veen, "Radio astronomical image formation using constrained least squares and Krylov subspaces," *Astronomy and Astrophysics*, 2016.

[10] C. L. Lawson and R. J. Hanson, *Solving least squares problems*. SIAM, 1974, vol. 161.

[11] J. Starck, E. Pantin, and F. Murtagh, "Deconvolution in astronomy: A review," *Publications of the Astronomical Society of the Pacific*, vol. 114, no. 800, p. 1051, 2002.

[12] B. Wakker and U. Schwarz, "The multi-resolution clean and its application to the short-spacing problem in interferometry," *Astronomy and Astrophysics*, vol. 200, pp. 312–322, 1988.

[13] T. J. Cornwell, "Multiscale clean deconvolution of radio synthesis images," *Selected Topics in Signal Processing, IEEE Journal of*, vol. 2, no. 5, pp. 793–801, 2008.

[14] R. Carrillo, J. McEwen, and Y. Wiaux, "Sparsity averaging reweighted analysis (SARA): a novel algorithm for radio-interferometric imaging," *Monthly Notices of the Royal Astronomical Society*, vol. 426, no. 2, pp. 1223–1234, 2012.

[15] R. E. Carrillo, J. D. McEwen, and Y. Wiaux, "PURIFY: a new approach to radio-interferometric imaging," *Monthly Notices of the Royal Astronomical Society*, vol. 439, no. 4, pp. 3591–3604, 2014.

[16] A. Leshem and A.-J. Van der Veen, "Radio-astronomical imaging in the presence of strong radio interference," *Information Theory, IEEE Transactions on*, vol. 46, no. 5, pp. 1730–1747, 2000.

[17] B. Ottersten, P. Stoica, and R. Roy, "Covariance matching estimation techniques for array signal processing applications," *Digital Signal Processing*, vol. 8, no. 3, pp. 185–210, 1998.

[18] S. J. Wijnholds, A.-J. van der Veen, F. De Stefani, E. La Rosa, and A. Farina, "Signal processing challenges for radio astronomical arrays," in *Acoustics, Speech and Signal Processing (ICASSP), 2014 IEEE International Conference on*. IEEE, 2014, pp. 5382–5386.

[19] P. E. Gill, W. Murray, and M. H. Wright, "Practical optimization," 1981.

[20] S. Foucart and D. Koslicki, "Sparse recovery by means of nonnegative least squares," *IEEE Signal processing Letters*, vol. 21, no. 4, pp. 498–502, 2014.

[21] J. A. Tropp and A. C. Gilbert, "Signal recovery from random measurements via orthogonal matching pursuit," *Information Theory, IEEE Transactions on*, vol. 53, no. 12, pp. 4655–4666, 2007.

[22] C. C. Paige and M. A. Saunders, "LSQR: An algorithm for sparse linear equations and sparse least squares," *ACM Transactions on Mathematical Software (TOMS)*, vol. 8, no. 1, pp. 43–71, 1982.

[23] C. A. Balanis, *Antenna theory: analysis and design*. John Wiley & Sons, 2016.

[24] A. R. Thompson, J. M. Moran, and G. W. Swenson Jr, *Interferometry and synthesis in radio astronomy*. John Wiley & Sons, 2008.